ORIGINAL PAPER

Shape and Size-Tailored Pd Nanocrystals to Study the Structure Sensitivity of 2-Methyl-3-butyn-2-ol Hydrogenation: Effect of the Stabilizing Agent

Lioubov Kiwi-Minsker · Micaela Crespo-Quesada

Abstract Uniform Pd nanocrystals of cubic, octahedral and cube-octahedral shapes were synthesized via a solution-phase method using two stabilizers: poly (vinyl pyrrolidone) (PVP) and di-2-ethylhexylsulfoccinate (AOT) and tested in the hydrogenation of 2-methyl-3-butyn-2-ol. The AOT-stabilized Pd nanocrystals were found to be an order of magnitude more active, but less selective than those stabilized by PVP. This could be attributed to a stronger interaction of PVP with surface Pd by adsorbed N-containing groups. The results obtained were rationalized applying a two-site Langmuir–Hinshelwood kinetic model that allowed predicting 3–4 nm cubic or octahedral nanocrystals stabilized by AOT as the optimum active phase ensuring the highest production rate of target MBE.

Keywords Palladium nanocrystals · Alkyne hydrogenation · Shape and size-controlled synthesis · Poly (vinyl pyrrolidone) (PVP) · Di-2-ethylhexylsulfoccinate (AOT) · Structure sensitivity

1 Introduction

The structure sensitivity of reactions catalyzed by metal nanocrystals has attracted considerable attention in the past few years [1–3]. The activity and selectivity of metal nanocrystals strongly depend on their surface morphology, i.e. on the relative amount of surface plane (Pd_{111} and Pd_{100}) and low coordination (edge and vertex) atoms. Pd catalyzed selective alkyne hydrogenations to alkenes are a particularly important type of structure sensitive reaction [4] since they are widely employed in the production of fine chemicals. Moreover, they are used in the complete elimination of alkynes from alkene feedstocks in industrial polymerization processes [5, 6].

Structure–sensitivity studies began primarily on single crystals [7–9]. However, these systems lacked the complexity normally present under industrial operation, in both the catalyst (material gap) and the reaction conditions (pressure gap). Model catalysts with well defined metal nanocrystals were thus developed [10–12], although the testing conditions used were still far from the real ones. With the development of simple preparation routes for obtaining size-controlled metal nanocrystals during the past decade [2, 3, 13, 14], along came numerous attempts to use such nanocrystals in structure–sensitivity studies under real operational conditions. On the other hand, the synthesis of shape-controlled metal nanocrystals was achieved more recently, and expanded the opportunities of research. However, the shape and size-controlled synthesis of Pd nanocrystals involves various growth-directing agents [2, 13, 14]. Despite the extensive post-synthesis cleaning procedures applied to the obtained nanocrystals, it is common to find traces of the stabilizing and capping agents which clearly modify the true catalytic behavior of the metal [15–17].

For acetylenic alcohol hydrogenations, the activity calculated per surface site (turnover frequency [TOF]) and the selectivity to the olefinic product were shown to increase with particle size [18–20]. Thus, atoms located on Pd_{111} were identified as the only active sites in the hydrogenation of 1,3-butadiene [11, 12] and 2-methyl-3-butyn-2-ol (MBY) [21, 22]. However, the Pd nanocrystals used in those studies possessed a very low percentage of Pd_{100} atoms on the surface [11, 12, 18, 21, 22], implying that their influence, albeit present, might have been overlooked.

L. Kiwi-Minsker (✉) · M. Crespo-Quesada
Group of Catalytic Reaction Engineering, Ecole Polytechnique Fédérale de Lausanne, 1015 Lausanne, Switzerland
e-mail: lioubov.kiwi-minsker@epfl.ch

Recently, research conducted in our group over well defined PVP-stabilized Pd nanocrystals showed that the semi-hydrogenation of MBY was indeed structure sensitive since two types of active sites were involved, namely plane (Pd_{111} and Pd_{100} surface atoms) and edge sites, with the former being fourfold more active [23]. Furthermore, over-hydrogenation to MBA occurred solely on the edge atoms.

Herein, we report the synthesis of uniform cubic, octahedral and cube-octahedral Pd nanocrystals of different sizes through a solution phase method using two stabilizers: PVP and AOT. The nanocrystals were tested in the water-assisted hydrogenation of MBY in order to elucidate the influence of stabilizing agents on catalytic response. The observed behavior was rationalized applying a two-site Langmuir–Hinshelwood kinetic model. Kinetic simulations predicted that ∼3 to 4 nm AOT-stabilized cubic or octahedra Pd nanocrystals should give the highest productivity of MBE.

2 Experimental Section

2.1 Catalyst Preparation

AOT-stabilized Pd nanocrystals were prepared in a reverse water/AOT/isooctane microemulsion [22]. Briefly, an aqueous solution of $PdCl_2(NH_3)_4$ (0.05 M) was used as metal precursor (pH 9, adjusted with ammonia), and a solution of hydrazine hydrate (3 M) as reducing agent to ensure complete reduction. Both solutions were then separately mixed with an isooctane solution of AOT (0.35 M) in order to prepare the microemulsions. Subsequently, both solutions were mixed and left to react for 1 h at room temperature. Isooctane was then evaporated in a rotary evaporator at 323 K, and the nanocrystals were purified from excess AOT by cyclic redispersion–centrifugation in methanol. The surfactant to metal ratio was changed in order to control the size of the nanocrystals.

PVP-stabilized Pd nanocrystals were synthesized according to previously published protocols [24, 25].

For cube-octahedral nanocrystals, 8.0 mL of an aqueous solution containing 105 mg of PVP and 60 mg of L-ascorbic acid were placed in a 25 mL vial, and pre-heated in air under magnetic stirring at 100 °C for 10 min. Then, 3.0 mL of an aqueous solution containing 57 mg Na_2PdCl_4 was added using a pipette. After the vial had been capped, the reaction was allowed to proceed at 100 °C for 3 h.

For cubic nanocrystals, 8.0 mL of an aqueous solution containing 105 mg of PVP, 60 mg of L-ascorbic acid, and 5 and 185 mg of KBr and KCl, respectively, were placed in a 20 mL vial and pre-heated in air under magnetic stirring at 80 °C for 10 min. Then, 3.0 mL of an aqueous solution containing 57 mg of Na_2PdCl_4 was added using a pipette.

The reaction was allowed to proceed at 80 °C for 3 h, after which the 6 nm nanocubes were collected by flocculation with acetone. In order to obtain 18 nm nanocubes, all reaction conditions were kept constant only that KBr was the only capping agent employed (600 mg).

For octahedral nanocrystals, they were prepared as follows: 3 mL of an aqueous Na_2PdCl_4 solution (9.5 mg/mL) was added into an aqueous solution (8 mL) containing 105 mg of PVP, 100 μL of CH_3CHO, and 0.3 mL of the Pd nanocubes (1.8 mg/mL, 18 nm in edge length) at 60 °C under magnetic stirring.

The final products were collected by centrifugation and washed with ethanol and water to remove excess PVP.

2.2 Catalyst Characterization

The morphology of the nanocrystals was analyzed by transmission electron microscopy (TEM), using a Philips CM20 microscope at 200 kV.

To determine the amount of Pd, the catalyst was dissolved in hot nitric acid and the sample was analyzed by atomic absorption spectroscopy via Shimadzu AA-6650 spectrometer with an air-acetylene flame.

2.3 Hydrogenation Experiments

The reactions were carried out in a baffled semi-batch stainless steel reactor (250 mL autoclave, Büchi AG, Switzerland) equipped with a heating jacket and a hydrogen supply system. An 8-blade disk turbine impeller was used as the stirrer. An appropriate amount of the Pd nanocrystals and 1 g of MBY were diluted with water up to 200 mL and sonicated for 5 min before introducing them into the reactor. After the reactor had been charged, it was flushed with N_2 and set to 60 °C. Subsequently, it was flushed with H_2 and pressurized to 0.3 MPa.

Samples were periodically withdrawn from the reactor and analyzed by GC analysis using an Auto System XL (Perkin Elmer) equipped with a 30 m Stabilwax (Crossbond Carbowax-PEG, Restek, USA) 0.32 mm capillary column with a 0.25 μm coating. The carrier gas (He) pressure was 101 kPa. The temperature of the Injector and the FID were 473 and 523 K, respectively. The oven temperature was held for 4 min at 323 K and then increased to 473 K at a rate of 30 K min^{-1}. The accuracy of the analysis was found to be of 0.1 wt% for all products.

3 Results and Discussion

3.1 Pd Nanocrystals

Figure 1 shows the AOT and PVP-stabilized Pd nanocrystals.

Fig. 1 TEM images of the samples used in this work. **a** PVP-stabilized small cubes (PCUB-6), **b** PVP-stabilized large cubes (PCUB-18), **c** PVP-stabilized octahedra (POCT-31), **d** PVP-stabilized cube-octahedra (PCOT-5.5), **e** AOT-stabilized small cube-octahedra (ACOT-5.5) and **f** AOT-stabilized large cube-octahedra (ACOT-11.5). For detailed structural information of the AOT-stabilized samples see Table 1
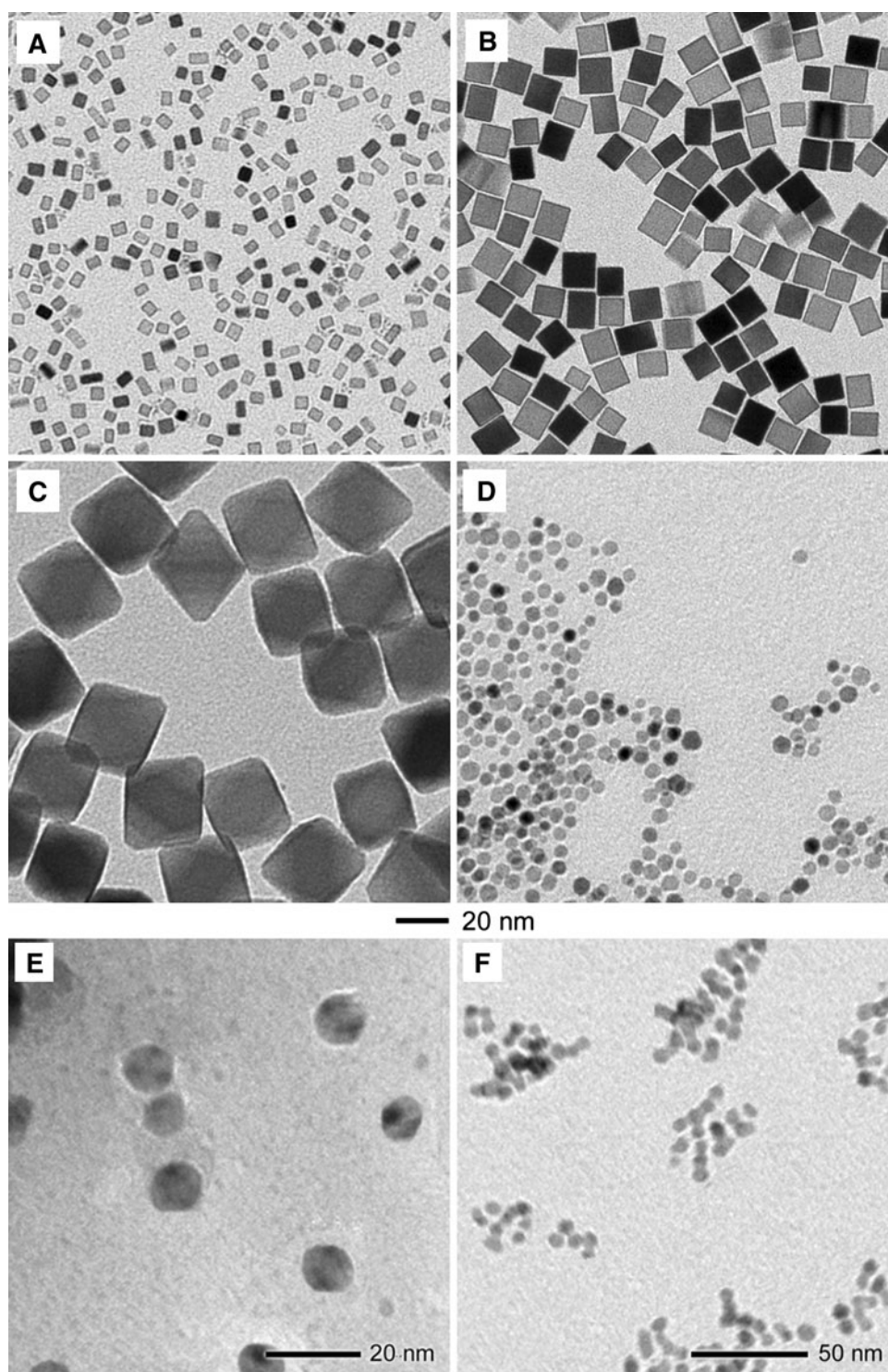
The surface statistics for ideal fcc nanocrystals performed by Van Hardeveld and Hartog [26] allow determining the relative amounts of different types of surface atoms on a nanoparticle of a particular size and shape. A more realistic model accounting for an incomplete outermost layer of surface atoms was employed. Table 1 gathers this information for the AOT-stabilized nanocrystals used in this study.

3.2 Water-Assisted Hydrogenation of MBY

In order to compare the catalytic behaviour of differently size and shaped nanocrystals, it is necessary to refer the measured activity (transformation rate of MBY) to the amount of surface atoms, obtaining the TOF:

**Table 1** Surface statistics of the nanocrystals used in this work

Sample	d_p (nm)	D^a (%)	x_{111}^b (%)	x_{100}^b (%)	x_{edge}^b (%)
ACOT-5.5	5.5	18.3	43.7	5.6	30.3
ACOT-11.5	11.5	9.2	60.6	11.8	16.6
PCUB-6	6	16.7	–	72.1	15.8
PCUB-18	18	6.0	–	90.0	6.0
POCT-31	31	3.6	93.2	–	5.5
PCOT-5.5	5.5	18.3	43.7	5.6	30.3

Estimated from [26]

[a] Dispersion (%), defined as the ratio of the number of surface atoms (N_S) to the total number of atoms (N_T)

[b] Percentage of surface atoms of a given type, $x_i = N_i/N_iN_S.N_S \cdot 100$

Scheme 1 Simplified reaction network for the hydrogenation of MBY based on a two site mechanism
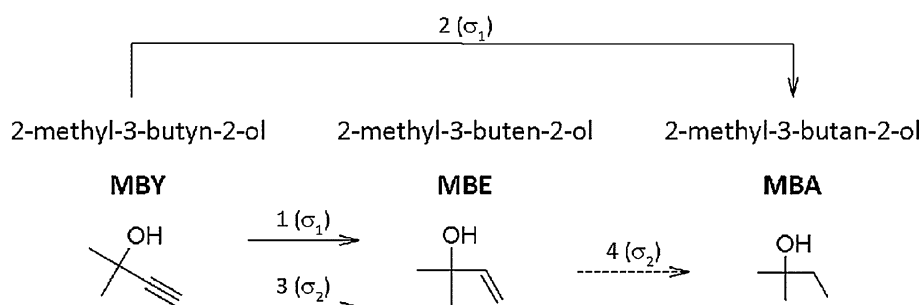
$$TOF[s^{-1}] = \frac{r\left[\frac{mol}{mol_{Pd}s}\right]}{D[-]} \quad (1)$$

where r is the observed reaction rate and D is the dispersion defined as in Table 1.

The structure–sensitivity of catalytic reactions is often studied by varying the size of near-spherical or cube-octahedral nanocrystals [11, 12, 18, 21, 22]. For these particles, the predominant type of plane atom is located on Pd_{111}, thus conveying the impression of being the active sites of the reaction. In order to verify this hypothesis, the water-assisted hydrogenation of MBY was carried out over PVP-stabilized Pd cubic (6 and 18 nm), octahedral (31 nm) and cube-octahedral (5.5 nm) nanocrystals [23]. All nanocrystals were active and selective thus demonstrating that Pd_{100} can indeed effectively hydrogenate MBY. Furthermore, the results suggested that the reaction took place on two active sites concomitantly. Indeed, Pd_{111} and Pd_{100}, or plane atoms, behaved similarly and were thus grouped as the first type of active site (σ_1). Low-coordination atoms, such as edge and corner atoms constituted the second type of active site (σ_2).

Indeed, a two-site Langmuir–Hinshelwood kinetic model allowed for an accurate description of the experimentally observed activity and selectivity. According to the reaction network shown in Scheme 1, the semi-hydrogenation was proposed to occur on both types of sites, but the reactivity depended on the coordination number of the atoms (*paths 1 and 3*). Edge atoms were fourfold less active in the semi-hydrogenation as compared to plane atoms. Direct over-hydrogenation to the alkane (*path 2*) occurred solely on plane atoms (σ_1) and the consecutive hydrogenation of MBE to MBA (*path 4*) on edge atoms (σ_2), presumably due to an increased adsorption strength of the alkene on the latter. The existence of parallel routes happening in different active sites in structure sensitive reactions and their influence on selectivity is a subject that has not hitherto been much discussed in the literature [26].

The observed activity of a catalyst could then be modeled with the following expression:

$$TOF_{obs} = TOF_{\sigma_1} \cdot x_{\sigma_1} + TOF_{\sigma_2} \cdot x_{\sigma_2} \quad (2)$$

where x_{σ_1} and x_{σ_2} refer to the fraction of plane and edge surface atoms, respectively.

The same approach was applied to the PVP and AOT-stabilized Pd nanocrystals in order to compare the results obtained with different stabilizing agents. Figure 2 shows a comparison of the observed TOFs as a function of nanoparticle dispersion for PVP and AOT-stabilized nanocrystals. The overall trend observed was the same, namely that TOF increased as dispersion decreases. This behaviour is referred to as antipathetic structure sensitivity, and it had already been observed for this reaction [22]. Nonetheless, the TOFs for the AOT-stabilized nanocrystals were sensibly higher than those for the nanocrystals stabilized by PVP. This trend had already been observed in the
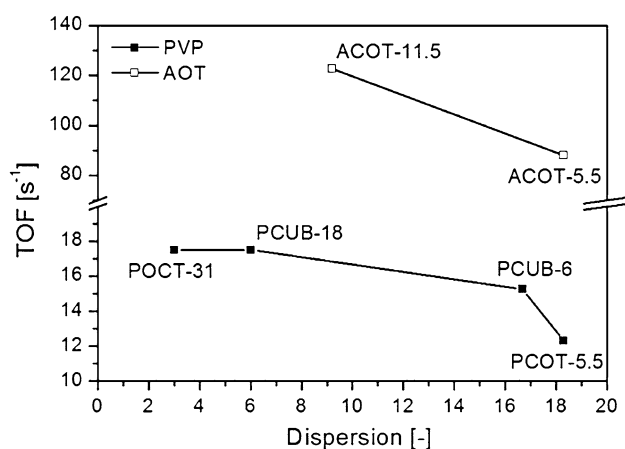
Fig. 2 Observed TOFs of the hydrogenation of MBY over PVP and AOT-stabilized nanocrystals as a function of dispersion. Reaction conditions: 1 g of MBY in 200 mL of water, 60 °C, 0,3 MPa of H_2 and 0,05 mg of Pd

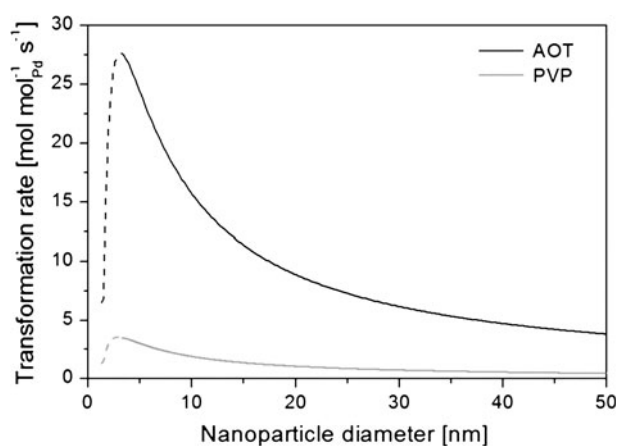**Fig. 3** Comparison of the expected activity for AOT and PVP-stabilized octahedral in the selective hydrogenation of MBY

hydrogenation of ethylene over TTAB and PVP stabilized nanocrystals and was attributed to a weaker interaction of TTAB with metal surfaces than PVP [27]. AOT can also be considered a weak stabilizer, since AOT-capped nanocrystals showed the same activity as CTAB-stabilized ones in the selective hydrogenation of MBY [21].

The specific σ_1 and σ_2 TOFs were subsequently estimated by solving Eq. (2) with a least squares approach, using the surface characteristics for each sample presented in Table 1. Table 2 gathers the values obtained for both PVP and AOT. It can be seen that the model could be successfully applied to the AOT-stabilized nanocrystals as well. Furthermore, plane atoms were also estimated to be more active than edge atoms for the semi-hydrogenation. This could be rationalized since the adsorption strength of the substrate on a given metal varies in the same order: aromatic < olefin < diolefin < alkyne [28]. This observation implies that an increase in the adsorption strength of the alkyne, such as adsorbing on an electronically deficient site (i.e. an edge atom) rather than on a plane atom, would reduce the activity, whereas an opposite trend would be observed for the olefin.

The joint application of the surface statistics of octahedral Pd nanocrystals together with the values for the specific TOF of plane atoms allows the comparison of the expected

activity in the hydrogenation of MBY for the aforementioned shape in the 3–50 nm size range, as shown in Fig. 3.

The selectivity towards the alkene was slightly influenced by the nature of the stabilizer, but not by the morphology of the nanocrystals. Indeed, all PVP-stabilized nanocrystals showed 95 % selectivity towards MBE at 50 % conversion, whereas for the AOT-stabilized nanocrystals, a value of 90 % was obtained for at the same conversion. This promoting effect of PVP could derive from its stronger interaction with the Pd nanocrystals. Promotion with N-containing molecules is usually rationalized by either a selective site blocking with respect to the alkene [29], or by a modification of the electronic properties of the nanocrystals [5, 30–32].

3.3 Nanoparticle Size and Shape Optimization

Activity was regarded as the optimization criterion since selectivity was not influenced to a great extent by the nature of the stabilizer. Thus, the determination of the specific TOFs for each type of active site for AOT-stabilized nanoparticles allows to model and predict the activity of hypothetical nanocrystals of a given size and shape, as it was done in Fig. 3 for octahedral nanoparticles. Figure 4 shows the predicted TOF and MBY transformation rates for three common nanoparticle shapes in the 3–50 nm range.

Naturally, the trend is the same than the one that was obtained for PVP-stabilized Pd nanocrystals [23]. The magnitudes, however, vary substantially. In this case, shape was also irrelevant as far as plane atoms are concerned. That is, cubes and octahedra are expected to show the same activity. Consequently, cubes or octahedra of roughly 3–4 nm are expected to be the most active nanoparticle for this application.
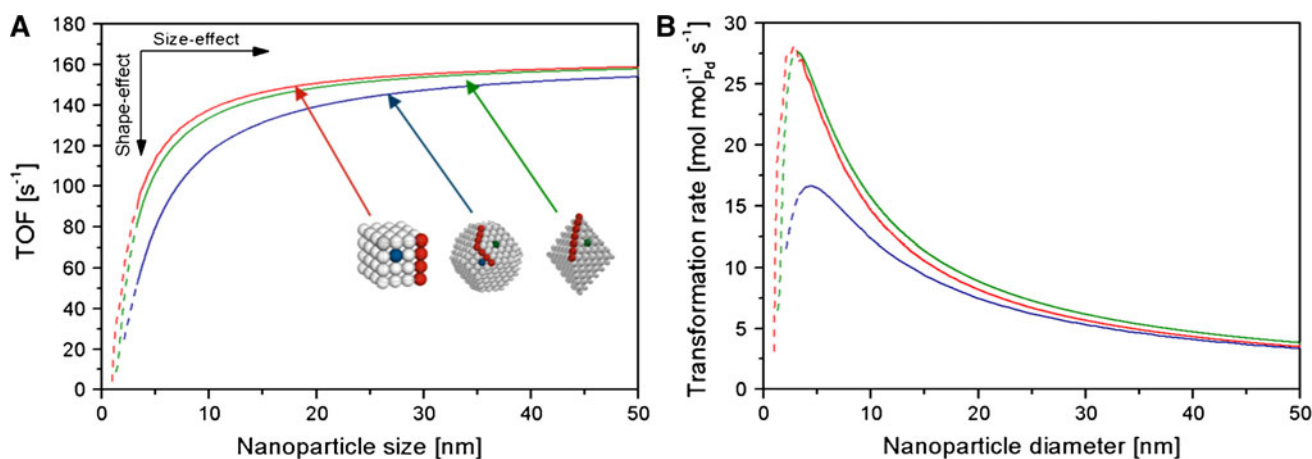
Table 2 Specific activity for σ_1 and σ_2 sites

Stabilizer	TOF$_{\sigma1}$ (s^{-1})	TOF$_{\sigma2}$ (s^{-1})
PVP	19.3 ± 2.4	4.7 ± 0.8
AOT	164.4 ± 0.05	22.9 ± 0.01

Reaction conditions 1 g of MBY in 200 mL of water, 60 °C, 0,3 MPa of H_2 and 0,05 mg of Pd

Fig. 4 Optimization of AOT-stabilized Pd nanocrystals' shape and size based on **a** TOF and **b** MBY transformation rate

4 Conclusions

Unsupported PVP-s and AOT-stabilized Pd nanocrystals of cubic, octahedral and cube-octahedral shapes of different sizes were tested in the water-assisted selective hydrogenation of MBY in order to reveal the effect exerted by the stabilizing agents. Indeed, Pd nanocrystals of the same shape and size stabilized by AOT were found to be an order of magnitude more active than those stabilized by PVP. This could be attributed to the stronger interaction of PVP with Pd surface atoms as compared to AOT. The results obtained were rationalized applying a two-site Langmuir–Hinshelwood kinetic model that allowed predicting 3–4 nm cubic or octahedral nanocrystals stabilized by AOT as the optimum active phase ensuring the highest production rate of target MBE.

References

1. Boudart M (1995) Chem Rev 95:661–666
2. Semagina N, Kiwi-Minsker L (2009) Catal Rev 51:147–217
3. Jia CJ, Schuth F (2011) Phys Chem Chem Phys 13:2457–2487
4. Boitiaux JP, Cosyns J, Robert E (1987) Appl Catal 32:145–168
5. Molnar A, Sarkany A, Varga M (2001) J Mol Catal A 173:185–221
6. Chen B, Dingerdissen U, Krauter JGE, Rotgerink HGJL, Mobus K, Ostgard DJ, Panster P, Riermeier TH, Seebald S, Tacke T, Trauthwein H (2005) Appl Catal A 280:17–46
7. Gunter PLJ, Niemantsverdriet JW, Ribeiro FH, Somorjai GA (1997) Catal Rev 39:77–168
8. Imbihl R, Ertl G (1995) Chem Rev 95:697–733
9. Zaera F (2001) Prog Surf Sci 69:1–98
10. Freund HJ (2008) Top Catal 48:137–144
11. Silvestre-Albero J, Rupprechter G, Freund HJ (2006) J Catal 240:58–65
12. Silvestre-Albero J, Rupprechter G, Freund HJ (2006) Chem Commun 80–82
13. Tao AR, Habas S, Yang PD (2008) Small 4:310–325
14. Xia Y, Xiong YJ, Lim B, Skrabalak SE (2009) Angew Chem 48:60–103
15. Habas SE, Lee H, Radmilovic V, Somorjai GA, Yang P (2007) Nat Mater 6:692–697
16. Quintanilla A, Butselaar-Orthlieb VCL, Kwakernaak C, Sloof WG, Kreutzer MT, Kapteijn F (2010) J Catal 271:104–114
17. Piccolo L, Valcarcel A, Bausach M, Thomazeau C, Uziob D, Berhault G (2008) Phys Chem Chem Phys 10:5504–5506
18. Wilson OM, Knecht MR, Garcia-Martinez JC, Crooks RM (2006) J Am Chem Soc 128:4510–4511
19. Zakarina NA, Zakumbaeva GD, Toktabaeva NF, Dyusenbina BB, Litvyakova EN, Kuanyshev AS (1983) Kinet Catal 24:733–737
20. Zakumbaeva GD, Zakarina NA, Naidin VA, Dostiyarov AM, Toktabaeva NF, Litvyakova EN (1983) Kinet Catal 24:379–383
21. Semagina N, Kiwi-Minsker L (2009) Catal Lett 127:334–338
22. Semagina N, Renken A, Laub D, Kiwi-Minsker L (2007) J Catal 246:308–314
23. Crespo-Quesada M, Yarulin A, Jin M, Xia Y, Kiwi-Minsker L (2011) J Am Chem Soc 133:12787–12794
24. Lim B, Jiang MJ, Tao J, Camargo PHC, Zhu YM, Xia YN (2009) Adv Funct Mater 19:189–200
25. Jin M, Liu H, Zhang H, Xie Z, Liu J, Xia Y (2011) Nano Res 4:83–91
26. Bond GC (1991) Chem Soc Rev 20:441–475
27. Lee H, Habas SE, Kweskin S, Butcher D, Somorjai GA, Yang PD (2006) Angew Chem 45:7824–7828
28. Hub S, Hilaire L, Touroude R (1988) Appl Catal 36:307–322
29. Nijhuis TA, van Koten G, Kaptejn F, Moulijn JA (2003) Catal Today 79–80:315–321
30. Sulman EM (1994) Rus Chem Rev 63:923–936
31. Mallat T, Baiker A (2000) Appl Catal A 200:3–22
32. Boitiaux JP, Cosyns J, Vasudevan S (1985) Appl Catal 15:317–326